Molecular Therapy
Methods & Clinical Development
Original Article

An Assay that Predicts *In Vivo* Efficacy for DNA Aptamers that Stimulate Remyelination in a Mouse Model of Multiple Sclerosis

Robin M. Heider,[1] John A. Smestad,[1,2] Hernan Nicolas Lemus,[3] Brandon Wilbanks,[1] Arthur E. Warrington,[3] Justin P. Peters,[1] Moses Rodriguez,[3] and L. James Maher III[1]

[1]Department of Biochemistry and Molecular Biology, Mayo Clinic College of Medicine and Science, 200 First Street SW, Rochester, MN 55905, USA; [2]Medical Scientist Training Program, Mayo Clinic College of Medicine and Science, 200 First Street SW, Rochester, MN 55905, USA; [3]Departments of Neurology and Immunology, Mayo Clinic College of Medicine and Science, 200 First Street SW, Rochester, MN 55905, USA

Multiple sclerosis (MS) is a debilitating disease for which regenerative therapies are sought. We have previously described human antibodies and DNA aptamer-streptavidin conjugates that promote remyelination after systemic injection into mice infected by Theiler's murine encephalomyelitis virus. Here, we report an *in vitro* assay of myelin binding with results that correlate with remyelination outcome *in vivo*, as shown for data from a set of DNA aptamer complexes of different size and formulation. This *in vitro* assay will be valuable for future screening of MS regenerative therapies targeting remyelination.

INTRODUCTION

Multiple sclerosis (MS) is a chronic, debilitating disease with prevalence as high as 0.1% in northern latitudes.[1] Although the cause of MS is largely unknown, the disease etiology is considered to be an immune-mediated attack on myelin, a specialized membrane that insulates nerves of the CNS. MS is characterized by CNS lesions accompanied by localized inflammation with common presenting symptoms of numbness, weakness, gait disturbances, and dizziness, with disability often accumulating over time.[1,2]

Modern treatments for MS address the immune response,[3] stimulate repair of existing lesions, or slow disease progression,[4] but no current therapies are considered curative. Disease progression and patient disability correlate with axonal damage,[5] and evidence suggests remyelination may partially protect neurological function.[6] Thus, a potential avenue to address current treatment disparities includes neuro-regenerative therapies exemplified by cell transfer of oligodendrocyte progenitors[7] or a recombinant human immunoglobulin M (IgM) autoantibody (rHIgM22) that has been shown to stimulate remyelination in multiple animal models of MS.[8] To address limitations associated with biologics, we have identified a DNA aptamer-based alternative that drastically reduces the size and synthetic cost of the stimulatory molecule. This DNA aptamer is the product of *in vitro* selection (SELEX) against murine myelin suspension as a selection target.[1] The myelin binding aptamer sequence of interest, 3064 (Figure 1A), is a guanosine-rich 40-nucleotide sequence characterized by G-quadruplex-forming secondary structures (Figure 1B).[9] When functionalized with a 3′ biotin tag and conjugated to streptavidin in a 4:1 molar ratio, the formulation (termed Myaptavin-3064, or 3064-BS here) exhibits myelin-regenerative properties in the Theiler's murine encephalomyelitis virus (TMEV) mouse model of MS,[10] a model characterized by chronic demyelination.[11]

Because streptavidin is a bacterial protein, the aptamer-streptavidin complex has the potential to be immunogenic in mammals, potentially limiting its therapeutic efficacy. This prompts the desire to identify other effective aptamer formulations. In the current work, we describe how the lack of activity of a rationally designed streptavidin-free aptamer-presenting DNA complex led to the observation that *in vitro* myelin binding is a surrogate for *in vivo* remyelination induction. Here, we describe the design of a rapid and reproducible myelin-binding assay and demonstrate its utility in qualifying novel alternative aptamer formulations by demonstrating the correlation between *in vitro* assay performance and *in vivo* remyelination.

RESULTS AND DISCUSSION

Preparation of Protein-Based and Protein-free Aptamer Complexes

Streptavidin-based conjugates studied here involve aptamer sequences shown in Figure 2A. 3′ biotinylated versions of each of these oligonucleotides were mixed in a 4:1 ratio to produce streptavidin-oligonucleotide conjugates (Figure 2B), as described previously.[10] Because streptavidin is a bacterial protein, with immunogenicity that may limit its therapeutic efficacy, we therefore sought to develop streptavidin-free aptamer formulations that could overcome this possible limitation.

Received 19 December 2017; accepted 17 March 2018;
https://doi.org/10.1016/j.omtm.2018.03.005.

Correspondence: L. James Maher III, PhD, Department of Biochemistry and Molecular Biology, Mayo Clinic College of Medicine, 200 First Street SW, Rochester, MN 55905, USA.
E-mail: maher@mayo.edu

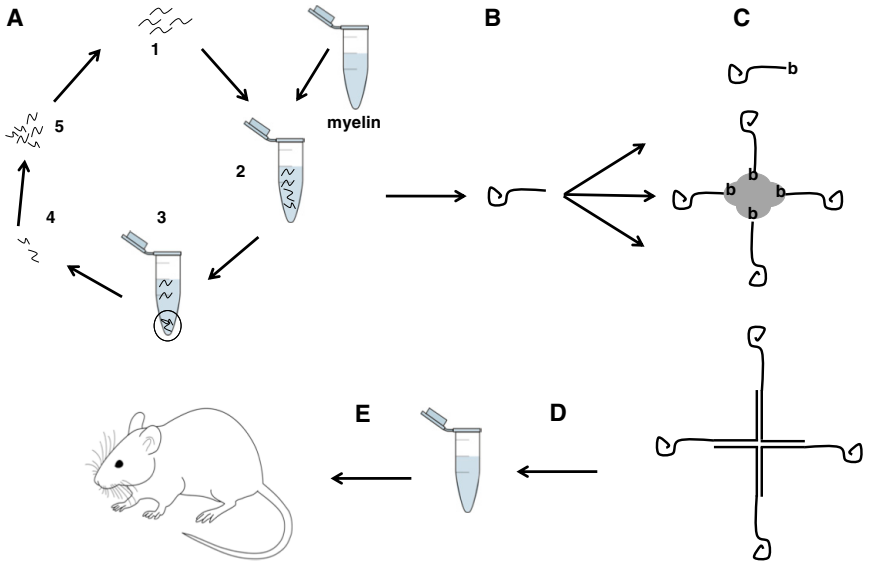

Figure 1. Background and Concept

(A) *In vitro* selection was previously used to identify a DNA aptamer sequence that preferentially binds murine myelin suspension: a DNA aptamer library (1, wavy lines) was exposed to murine myelin suspension (2), and centrifugation was utilized to isolate aptamers bound to the myelin pellet (3). Sequences associated with murine myelin were purified (4), amplified using PCR (5), and one strand of each duplex of the library used in subsequent selection rounds until a sequence becomes significantly enriched in the resulting pool of oligonucleotides. (B) *In vitro* selection yielded anti-myelin DNA aptamer (3064) encoding a G-quadruplex secondary structure (hooked line). (C) The anti-myelin DNA aptamer has been formulated in different ways for testing. These include free biotinylated DNA (top), conjugates with streptavidin (middle), and protein-free base-paired four-way-junction assemblies (bottom). (D and E) Anti-myelin aptamer formulations can be tested in an *in vitro* myelin binding assay (D), with the hypothesis that the degree of myelin binding *in vitro* predicts remyelination properties in mouse models of MS (E).

We designed protein-free multivalent aptamer candidates using NUPACK software,[12] leveraging principles of catalytic hybridization to achieve a dynamic structural equilibrium favoring assembly of aptamer-presenting four-way-junction cruciform structures ("4WJ"). This approach was inspired by previously published work demonstrating programmed biomolecular self-assembly of oligonucleotide systems.[13] The design of our programmed biomolecular self-assembly process involved a system of metastable aptamer-presenting hairpin structures (Figure 2D), which can be triggered to sequentially hybridize into higher order complexes (Figure 2E) by the addition of an initiator oligonucleotide (Figure 2C). Versions of protein-free multivalent aptamer 4WJ candidates were also be synthesized with locked nucleic acid modified sugars at 5′ and 3′ termini (Figure S1; "3064-4WJ-LNA") to reduce susceptibility to exonuclease degradation and potentially extend serum half-life.[14]

For the previously described streptavidin-aptamer conjugates, conjugation was analyzed by native acrylamide gel electrophoresis revealing a mixture of complexes, dependent on the sequence and folding of the biotinylated aptamers (Figure 3A). 3064 assembly was compared with a second G-rich DNA sequence (3060; Figures 2A and 3A) that does not bind myelin and a T_{40} negative control DNA sequence (3202; Figures 2A and 3A). All sequences were functionalized with a 3′ biotin tag and a 5′ 6-FAM for visualization. Consistent with our previous work, the results suggest a heterogeneous ensemble of complexes with 1–4 aptamers per streptavidin tetramer.

Protein-free aptamer conjugate assembly was analyzed using agarose gel electrophoresis (Figures 3B and 3C). Stepwise isothermal assembly of multiple hairpin structures into a higher order complex was confirmed, as was the dependence of complex assembly on the presence of the initiator oligonucleotide. Additionally, the prepared protein-free aptamer complexes were observed to be prepared with relatively high homogeneity.

In Vivo Testing of Protein-free Aptamer Formulations

Protein-free complexes 3064-4WJ and 3064-4WJ-LNA were tested in the TMEV mouse model of MS to assess whether either of these reagents possesses remyelination-stimulating properties that are comparable to streptavidin-based formulations. Chronically TMEV-infected mice (>180 days post-infection) were dosed with protein-free aptamer formulations and remyelination scores calculated, comparing to streptavidin-based aptamer formulations and buffer control. Remyelination scores following treatment (Table 1) indicate that neither 3064-4WJ nor 3064-4WJ-LNA was as effective at stimulating remyelination as streptavidin-based complex 3064-BS, though both 3064-4WJ and 3064-4WJ-LNA were more effective than 3064-B. Statistical analysis suggests no significance in efficacy between 3064-B and 3064-4WJ or 3064-4WJ-LNA (Table 1). This failure of a rationally designed protein-free multivalent aptamer formulation indicates the complexity of designing remyelinating agents. We hypothesized that the failure of protein-free 3064-4WJ and 3064-4WJ-LNA related either to reduced biodistribution properties or reduced myelin binding affinity. We therefore investigated whether significant differences exist in these parameters that would explain the failure of these agents in *in vivo* remyelination experiments. The results inspired us to identify an *in vitro* assay that could be deployed during formulation development for prediction of *in vivo* remyelinating activity.

Pharmacokinetics of Protein-Based and Protein-free Aptamer Formulations

Using a previously devised qPCR method,[15] we assessed whether protein-free anti-myelin aptamer formulations 3064-4WJ and 3064-4WJ-LNA demonstrate biodistribution and pharmacokinetic properties similar to streptavidin-aptamer conjugates (3064-BS) or unconjugated biotinylated aptamer (3064-B). Measured serum levels suggest that protein-free aptamer formulations reach the circulation

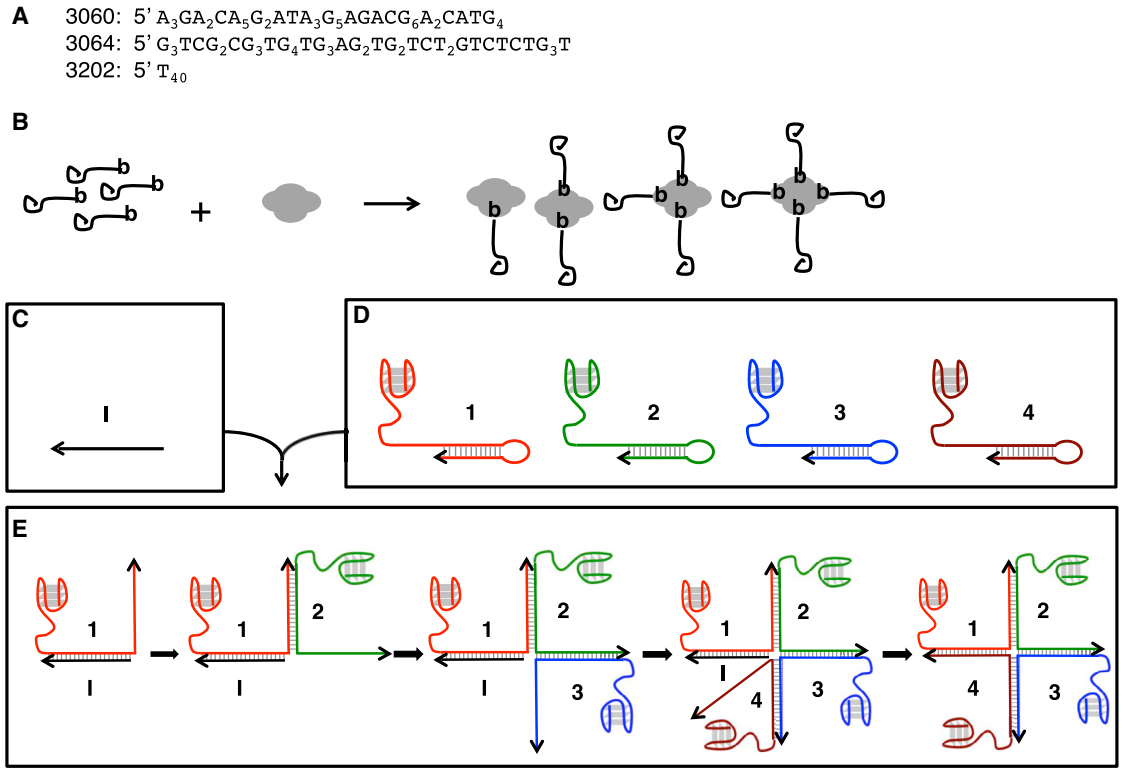

Figure 2. Aptamers Used in These Studies

(A) Ni-NTA-specific aptamer 3060 sequence capable of G-quadruplex formation; myelin-specific 3064 (derived from the sequence selected against murine myelin suspension); negative control homopolymer 3202. (B) Visualization of biotinylated aptamer-streptavidin conjugates is shown. Aptamers modified by 3′ biotin-TEG are mixed in a 4:1 molar ratio with streptavidin to create a mixed population of streptavidin-aptamer conjugates. (C and D) A short initiator sequence (C) is used to facilitate protein-free complex assembly involving four unique DNA sequences (D) that contain the 3064 aptamer sequence in addition to complementary hairpin sequences. (E) The initiator disrupts the hairpin structure of the sequence 1, exposing a free stretch of DNA complementary to one of the hairpin forming strands of 2, etc., promoting formation of the desired tetrameric complex (1 + 2 + 3 + 4).

following intraperitoneal injection (Figure 4, right) and gain access to the CNS, suggesting they can reach myelin targets *in vivo* (Figure 4, left and middle panels).

To evaluate whether altered biodistribution influenced the observed difference in therapeutic activity between formulations, we quantitated area under the curve (AUC) using the gamma variate summation model to characterize tissue exposure. We found that AUC values were comparable between each formulation in brain. Biodistribution varied among formulations in spinal cord (Table 2; Figure S2), with 3064-4WJ and 3064-B having greater exposure than 3064-4WJ-LNA and 3064-BS. These trends in biodistribution do not explain the observed remyelination scores (Table 1), where 3064-BS exhibited pronounced remyelination activity compared to the other formulations. Likewise, the difference in tissue exposure of 3064-4WJ and 3064-4WJ-LNA does not explain their similar remyelination scores. This suggests that the observed biological responses in the remyelination experiment are not solely determined by tissue exposure. We hypothesized that remyelination activity may also reflect target binding activity. We investigated this hypothesis using a novel *in vitro* myelin binding assay.

In Vitro Myelin Binding Assay

We developed a method that recapitulates the original myelin binding selection used to identify remyelinating aptamer 3064. In this method, fluorescein-tagged aptamer samples are incubated with sonicated murine myelin suspensions, followed by separation of bound and unbound aptamer fractions by centrifugation. The resulting myelin pellet is washed prior to re-suspension in PBS (Figure S3), and the fraction of aptamer fluorescence in the bound fraction is measured (Figure 5). This approach controls for potential differences in 5′ 6-FAM labeling efficiency at the time of synthesis and for known heterogeneity among different aptamer complexes. We calculated the effect size of myelin binding relative to 3064-B. Intriguingly, streptavidin-aptamer complex 3064-BS exhibited the greatest myelin binding, with the other protein-based aptamer formulations each showing reduced levels of myelin binding (i.e., negative effect sizes; Table 1). The protein-free aptamer formulations displayed positive effect sizes but smaller in magnitude than 3064-BS (Table 1). When comparing

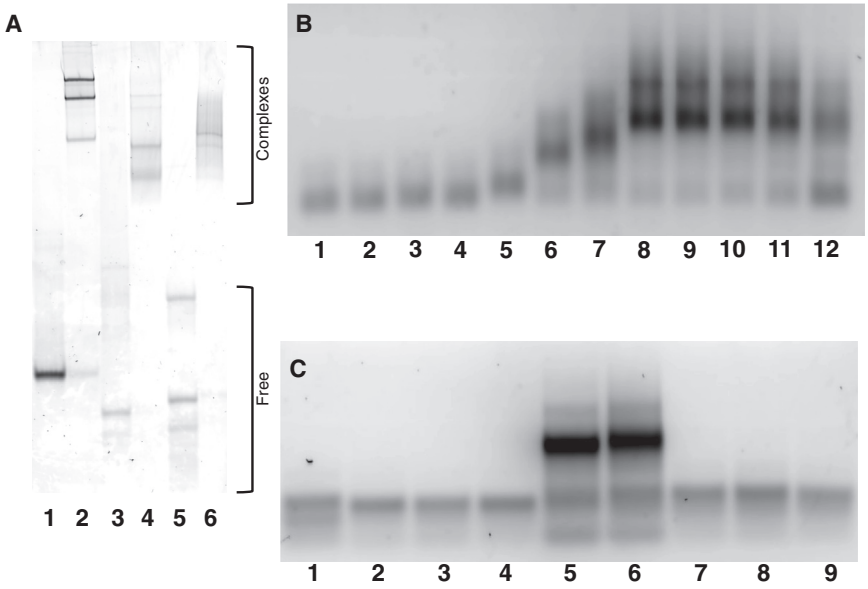

Figure 3. Assembly of Aptamer Formulations

(A) 8% native polyacrylamide gel stained with SYBR Gold to illustrate aptamer-streptavidin complex formation. Band patterns illustrate mixed population of complexes free aptamer and streptavidin complexed with 1–4 aptamers. Lane 1, 1 μM biotinylated 3202 alone; lane 2, 1 μM biotinylated 3202 with 0.25 μM streptavidin; lane 3, 1 μM biotinylated LJM-3060B alone; lane 4, 1 μM biotinylated 3060 with 0.25 μM streptavidin; lane 5, 1 μM biotinylated 3064 alone; lane 6, 1 μM biotinylated 3064 with 0.25 μM streptavidin. (B) 2% agarose gel stained with ethidium bromide demonstrating protein free-aptamer complex assembly optimization is shown (see Figure 2 for identities). Lane 1, D2; lane 2, D3; lane 3, D4; lane 4, D1; lane 5, I + D1; lane 6, I + D1 + D2; lane 7, I + D1 + D2 + D3; lane 8, I + D1 + D2 + D3 + D4 (1 equivalent I); lane 9, I + D1 + D2 + D3 + D4 (0.5 equivalent I); lane 10, I + D1 + D2 + D3 + D4 (0.25 equivalent I); lane 11, I + D1 + D2 + D3 + D4 (0.1 equivalent I); lane 12, D1 + D2 + D3 + D4. (C) 2% agarose gel stained with ethidium bromide demonstrating modified protein-free aptamer complex assembly using 0.1 molar equivalent I is shown (see Figure 2 for identities). Lane 1, D1 with 5′ 6-FAM modification; lane 2, D2, lane 3, D3; lane 4, D4; lane 5, D1 + D2 + D3 + D4 (0.1 equivalent I); lane 6, D1 with 5′ 6-FAM modification + D2, D3, and D4 with 3′ and 5′ locked nucleic acid modified sugars (0.1 equivalent I); lane 7, D2 with 3′ and 5′ locked nucleic acid modified sugars; lane 8, D3 with 3′ and 5′ locked nucleic acid modified sugars; lane 9, D4 with 3′ and 5′ locked nucleic acid modified sugars.

the two highest scoring formulations from this assay, 3064-BS and 3064-4WJ-LNA using a Tukey contrast test, a statistically significant difference exists ($p = 1.68e{-}5$). This suggests that myelin binding may be a surrogate for *in vivo* remyelination and that reduced myelin binding may explain the failure of protein-free aptamer formulations 3064-4WJ and 3064-4WJ-LNA to promote remyelination in animal experiments.

Correlation of *In Vitro* Myelin Binding and *In Vivo* Remyelination

We thus hypothesized that *in vitro* myelin binding of an aptamer formulation corresponds with remyelinating activity *in vivo*. Indeed, analysis of our data shows this to be the case. *In vivo* remyelination scores for each aptamer formulation plotted against the fraction bound to myelin *in vitro* revealed a strong correlation (0.83; p value: 0.02; Figure 6A). We conclude that this simple *in vitro* myelin binding assay serves as a valuable screening tool capable of prioritizing aptamer formulation candidates for future *in vivo* studies.

Deviations from expected remyelination scores based on the correlation plot are expected to be influenced by differential tissue exposure *in vivo*. For example, AUC values in spinal cord tissue are different between formulations, with greater exposure to 3064-4WJ relative to 3064-4WJ-LNA and 3064-BS (Figure S2). Although 3064-4WJ exhibited lower affinity to myelin *in vitro* relative to 3064-4WJ-LNA (Table 1), 3064-4WJ-LNA did not reach spinal cord tissue to the same extent as 3064-4WJ (Figure S2), resulting in similar remyelination scores. Conversely, although 3064-BS displayed lower spinal cord

Table 1. Comparison of *In Vivo* Remyelination Score and *In Vitro* Myelin Binding Assay Result for DNA Aptamer Formulations

Formulation	Remyelination *In Vivo*	SEM	p Value Relative to 3064-B	Fraction Bound *In Vitro*	SD[a]	Effect Size Relative to 3064-B	p Value Relative to 3064-B
3064-B	8.5[b]	3.4[b]	–	0.085	0.012	0	–
3064-BS	34.9[b]	6.1[b]	0.0039	0.194	0.027	8.69	<0.001
3060-B	10.3[b]	3.4[b]	0.9997	0.052	0.004	−2.64	<0.001
3060-BS	8.5[b]	4.5[b]	0.9999	0.026	0.002	−4.71	<0.001
3202-B	not tested	–	–	0.010	0.001	−6.04	<0.001
3202-BS	4.2[b]	2.3[b]	0.9863	0.026	0.004	−4.73	<0.001
3064-4WJ	14.0	6.0	0.9189	0.108	0.013	1.83	0.0048
3064-4WJ-LNA	13.3	4.8	0.9692	0.160	0.021	6.01	<0.001

[a]SD for n = 9 *in vitro* measurements.
[b]Data previously published.[10]

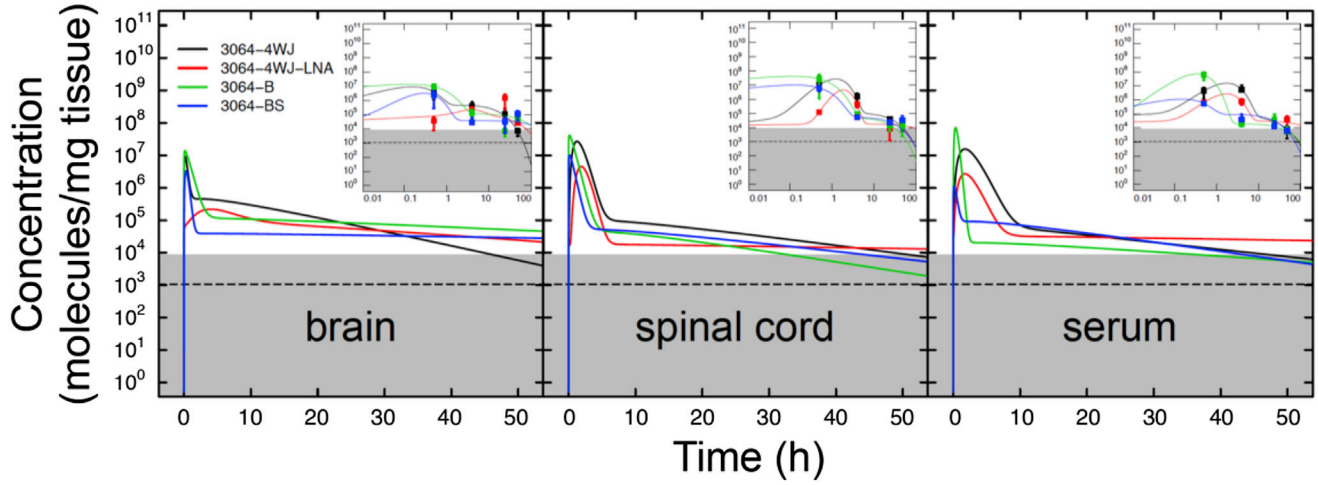

Figure 4. Pharmacokinetics of Aptamer Formulations in Mice

Mice were injected intraperitoneally with 1 μM aptamer solution (500 μL) and sacrificed at varying time points. After extensive perfusion, tissues were harvested and aptamer samples extracted and quantified by qPCR. Gamma variate pharmacokinetic fits of recovered aptamer (molecules per mg tissue) from the indicated tissues are plotted on a logarithmic scale as a function of time after intraperitoneal injection. The inset plots, with time in hours on a logarithmic scale for clarity, show the mean and SD for four determinations of aptamer concentrations calculated from qPCR trials using methods previously described.[15] Horizontal dashed line indicates median background signal from negative control qPCR quantitation with error bounds (gray region). Background in individual qPCR experiments from different mice at different time points and different tissues was pooled to show the variation observed.

tissue exposure relative to other formulations, its increased myelin affinity resulted in greater remyelination activity. Therefore, we corrected the remyelination score for the effect of spinal cord tissue exposure, i.e., AUC relative to 3064-BS. The results revealed an even stronger correlation (0.96; p value: 0.04; Figure 6B). Thus, optimization of both tissue exposure and myelin affinity is required for maximal remyelination *in vivo*.

Our observation of a correlation between apparent myelin binding affinity *in vitro* and stimulated remyelination *in vivo* gives some insight into the currently unknown mechanism of DNA aptamers that provoke myelin regeneration. It is reasonable to hypothesize that some molecular feature of myelin, perhaps an exposed epitope of a protein, such as myelin basic protein, is recognized by anti-myelin aptamers. The probability and duration of binding and cross-linking of such targets by multivalent aptamer complexes is enhanced by higher affinity. How cross-linking of such targets then signals a regenerative response to oligodendrocytes remains unknown.

Future experiments will also seek to understand how the structural differences between the 3064-BS protein conjugate and the protein-free 3064-4WJ formulations account for altered myelin binding affinity. For example, the 4WJ series formulations are characterized by a rigid and negatively charged core, quite different from the streptavidin core of BS series formulations.

MATERIALS AND METHODS

Aptamer-Streptavidin Conjugate Assembly

DNA aptamer oligonucleotides were synthesized by Integrated DNA Technologies (Coralville, IA) with 3′ biotin- triethylene glycol (TEG) modifications. Fluorescent aptamers were functionalized with an additional 5′ 6-FAM fluorescein modification. Oligonucleotide stock concentrations were determined using a spectrophotometer with molar extinction coefficients estimated by the manufacturer. Negative control oligonucleotide sequences are identified using number codes 3060 and 3202.

Streptavidin purchased from Genscript (Piscataway, NJ; Z02043-5; 5 mg) was re-suspended in 1 mL PBS. Concentration (mg/mL) was estimated by dividing the A_{280} value (measured using a Nanodrop 100 spectrophotometer) by a factor of 3.2. Molar concentrations were then calculated using the molecular weight of tetrameric streptavidin (54 kDa).

A solution of 1 μM aptamer carrying 3′ biotin-TEG modification in PBS supplemented with 1 mM $MgCl_2$ was incubated in an 85°C water bath for 5 min to disrupt secondary structures and snap cooled on ice for 15 min. A volume of streptavidin solution was added to a final streptavidin concentration of 0.25 μM, giving a 4:1 molar ratio of aptamer to streptavidin. The aptamer:streptavidin solution was mixed and incubated at 37°C for 1 hr to allow conjugate assembly. The distribution of conjugated species was assessed by electrophoresis through 8% native polyacrylamide (29:1 acrylamide: bisacrylamide) gel at 10 V/cm in 0.25× Tris/borate/EDTA (TBE) buffer. Gels were stained for 1 hr with 1× SYBR Green dye solution in 0.25× TBE buffer and imaged using a Typhoon FLA 7000 imager. Here, complexes are described using codes 3064-BS, 3060-BS, and 3202-BS whereas free biotinylated aptamers are described using codes 3064-B, 3060-B, and 3202-B.

Table 2. Aptamer Distribution Parameters from Fitting with Gamma Variate Summation Model

Formulation	k_1 (Molecules/ mg Tissue)	k_2 (Molecules/ mg Tissue)	a_1 (Dimensionless)	a_2 (Dimensionless)	b_1 (min)	b_2 (min)	$A(\infty)$ (min-Molecules/ mg Tissue)
Brain							
3064-4WJ	$1.9 + 1.6 \times 10^7$	$9.5 + 2.0 \times 10^5$	0.70 ± 0.25	3.1 ± 2.4	8.6 ± 1.4	380 ± 250	$6.9 \pm 1.4 \times 10^8$
3064-4WJ-LNA	$1.1 \pm 0.4 \times 10^5$	$8.5 \pm 0.9 \times 10^4$	0.24 ± 0.05	6.9 ± 0.4	56.0 ± 8.4	1,700 ± 100	$2.5 \pm 0.2 \times 10^8$
3064-B	$4.6 \pm 1.1 \times 10^7$	$1.6 \pm 0.3 \times 10^5$	1.20 ± 0.97	13.0 ± 2.8	11.0 ± 4.5	2,000 ± 600	$1.1 \pm 0.2 \times 10^9$
3064-BS	$1.1 \pm 0.4 \times 10^7$	$4.4 \pm 0.9 \times 10^4$	0.58 ± 0.21	37.0 ± 8.0	7.6 ± 0.9	8,400 ± 2,600	$7.4 \pm 2.8 \times 10^8$
Spinal Cord							
3064-4WJ	$2.0 \pm 0.9 \times 10^7$	$1.6 \pm 0.3 \times 10^5$	0.34 ± 0.15	3.3 ± 0.6	15.0 ± 4.9	710 ± 80	$8.8 \pm 2.2 \times 10^9$
3064-4WJ-LNA	$4.2 \pm 3.1 \times 10^5$	$1.9 \pm 0.4 \times 10^4$	0.22 ± 0.17	36.0 ± 9.4	23.0 ± 9.2	8,200 ± 2,700	$4.6 \pm 1.6 \times 10^8$
3064-B	$7.4 \pm 3.1 \times 10^7$	$6.2 \pm 3.2 \times 10^4$	1.20 ± 1.54	6.0 ± 3.6	15.0 ± 4.9	1,000 ± 300	$2.4 \pm 0.8 \times 10^9$
3064-BS	$1.6 \pm 0.4 \times 10^7$	$5.9 \pm 0.5 \times 10^4$	2.90 ± 2.50	4.9 ± 0.2	20.0 ± 3.8	1,200 ± 50	$5.8 \pm 1.0 \times 10^8$
Serum							
3064-4WJ	$2.6 \pm 0.7 \times 10^7$	$1.1 \pm 0.5 \times 10^5$	0.51 ± 0.10	80.0 ± 21.7	58.0 ± 14.4	840 ± 210	$2.9 \pm 0.9 \times 10^9$
3064-4WJ-LNA	$2.6 \pm 1.0 \times 10^6$	$4.8 \pm 4.6 \times 10^4$	0.30 ± 0.12	25.0 ± 18.1	30.0 ± 10.3	4,600 ± 1,100	$7.0 \pm 1.6 \times 10^8$
3064-B	$1.2 \pm 0.3 \times 10^8$	$3.1 + 0.4 \times 10^4$	0.32 ± 0.06	5.9 ± 1.7	6.1 ± 0.5	1,300 ± 300	$2.7 \pm 0.6 \times 10^9$
3064-BS	$1.9 \pm 0.4 \times 10^6$	$1.1 \pm 0.2 \times 10^5$	0.70 ± 0.24	3.1 ± 0.6	10.0 ± 1.2	640 ± 20	$1.2 \pm 0.1 \times 10^8$

$A(\infty)$ is area under the curve.
Fitting is to the following model:

$$C(t) = k_1 \left(\frac{\ln 2}{b_1} t\right)^{\frac{\ln 2}{a_1}} e^{-\frac{\ln 2}{b_1} t} + k_2 \left(\frac{\ln 2}{b_2} t\right)^{\frac{\ln 2}{a_2}} e^{-\frac{\ln 2}{b_2} t}.$$

Protein-free Complex Assembly

Hairpin-forming oligonucleotide sequences for protein-free complexes with and without modified locked nucleic acid bases (4WJ and 4WJ-LNA, respectively) were designed[12] using NUPACK 3.0. Standard DNA oligonucleotide sequences were synthesized by IDT. Sequences containing locked-nucleic acid modifications were synthesized by Exiqon (Germantown, MD) at 1 μmol scale. One oligonucleotide was synthesized by IDT with a 5′ 6-FAM modification. Oligonucleotides were received from the manufacturers as lyophilized pellets and suspended in water to approximate 1 mM concentrated stock solutions. Prior to complex assembly, each hairpin-forming oligonucleotide was diluted 1:100 in water, and the absorbance was measured at 260 nm using a Nanodrop 100 spectrophotometer. Beer's law was used to calculate actual concentrations, and 2.4-μM working stocks were created. The hairpin-forming oligonucleotides were folded by incubating in a slow-cooling water bath from 94°C to room temperature over 2 hr. The folded oligonucleotides were combined in equimolar concentrations (final concentration of 0.55 μM) with one-tenth molar equivalent initiator oligonucleotide and incubated for 3 hr at 37°C. Each assembly reaction was analyzed on a 2% agarose gel with 1× Tris/acetate/EDTA (TAE) buffer containing ethidium bromide. Electrophoresis was at 130 V for 50 min. DNA bands were visualized by scanning gel on Typhoon fluorimeter using fluorescence filters in ethidium bromide mode.

In Vivo Remyelination in the TMEV Mouse Model

Spinal cord morphometry and remyelination data in TMEV-infected mice compare previously published experiments (3064-BS, 3064-B, 3060-BS, 3060-B, 3202-BS, and 3202-B)[10] and new experiments (3064-4WJ, 3064-4WJ-LNA, and PBS) performed by the methods previously described.[10] All studies conformed to Mayo Clinic and NIH animal use guidelines and were reviewed and approved by the Mayo Clinic Institutional Animal Care and Use Committee as protocol A29509.

Eight-week-old female Swiss Jim Lambert (SJL/J) mice experienced demyelination by 6 months of chronic TMEV infection. Groups of 6–10 mice received 500 μL intraperitoneal injections of the various aptamer formulations (1 μM final concentration of aptamer) in Calcium-free D-PBS (Invitrogen) supplemented with magnesium chloride (1 mM). Injections were twice per week for 5 weeks. Mice were euthanized with sodium pentobarbital and perfused intracardially with Trump's fixative (phosphate-buffered 4% formaldehyde/1% glutaraldehyde [pH 7.4]). Spinal cords were removed, cut into 1 mm blocks, and every third block fixed and stained with osmium tetroxide and embedded in araldite plastic (Polysciences, Warrington, PA). One-micrometer-thick cross-sections were cut from each block, mounted onto glass slides, and stained with 4% paraphenylenediamine to visualize myelin.[10] Cross-sections (10–12) represent samples from the cervical, thoracic, lumbar, and sacral spinal cord. Neuropathology to characterize extent of lesion remyelination was

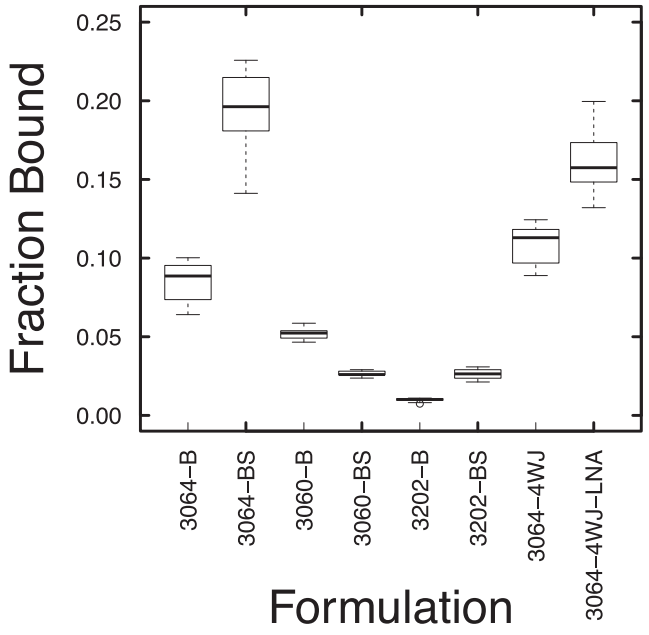

Figure 5. Fraction of Aptamer Sample Associated with Myelin Pellet in a Binding Assay

Fluorescent counts were measured from the re-suspended pellet, supernatant, and washes. The fluorescent counts measured from the re-suspended pellets were divided by the sum of all fluorescent counts for each sample. Three independent biological replicates of each formulation were tested in three separate trials before pooling "fraction bound" values (n = 9). Error bars indicate SEM.

performed according to a blinded protocol. Slides were first coded by numbers and then randomized across all experimental groups such that slides from one animal were not grouped consecutively together but appeared to the examiner for grading in a blinded and random manner. Two investigators (M.R. and A.E.W.) examined the sections independently. For grading, each spinal cord section was divided visually into four quadrants based on morphological symmetry of the coronal section and examined by bright-field microscopy at 100× and 200× total magnification using an Olympus Provis microscope. Demyelinated areas were characterized by denuded axons and inflammatory cell infiltrates. In contrast, demyelinated areas with remyelination were characterized by thin myelin sheaths compared with the thicker, intact myelin sheaths. The spinal cord white matter was scored as normal, demyelinated with no remyelination, or demyelinated with remyelination.[10] Partial quadrants were excluded. Lesions were judged to be remyelinated when the lesion was 75%–100% repaired. Remyelinated lesions below this threshold were scored as negative. Data were not assembled into treatment groups until all slides in a given study were graded. Demyelination for each mouse was calculated as a percentage based on the number of spinal cord quadrants with demyelination, which includes those quadrants with demyelination and repair, divided by the total number of quadrants scored. Remyelination for each mouse was calculated as a percentage based on the number of demyelinated quadrants above threshold remyelination divided by the number of quadrants with demyelination. Data for percentage spinal cord demyelination and remyelination were compared. p values were calculated by performing one-way ANOVA with multiple comparisons using Graphpad Prism 7.0a for Mac OSX (GraphPad, La Jolla, CA, USA; https://www.graphpad.com).

Pharmacokinetics of Protein-free and Protein-Based Aptamer Complexes in Mice

Pharmacokinetic measurements were made as previously described.[15] Four mice were included for each time point, with one mouse left untreated as a negative control. Aptamer administration, tissue preparation, aptamer extraction, and qPCR were performed as previously described,[15] and the pharmacokinetic modeling results are given in Table 2. Parameter estimates are reported from pharmacokinetic modeling along with uncertainty estimates from fitting 1,000 simulated datasets as previously described.[15] Total tissue exposure to aptamer was estimated by AUC analysis.

Myelin Binding Assay

Murine myelin was prepared from SJL mice as previously described.[10] The *in vitro* myelin binding activities of different aptamer

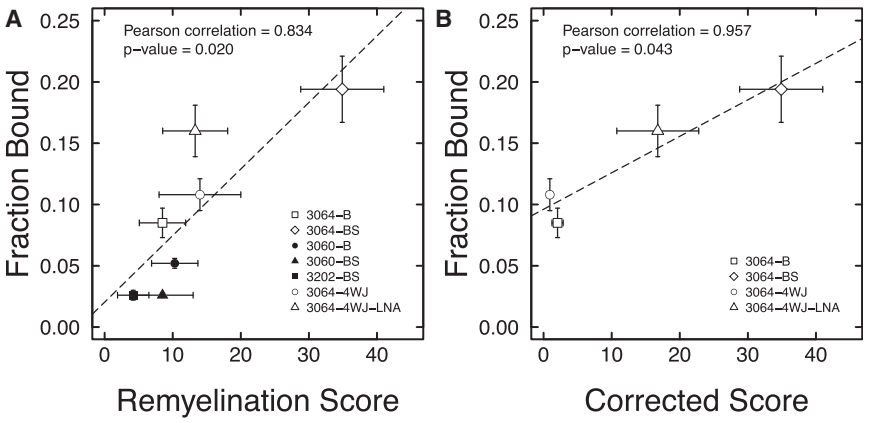

Figure 6. Relationship between Aptamer Binding to Myelin *In Vitro* and Remyelination Stimulation *In Vivo*

(A) Remyelination scores from *in vivo* studies are plotted against fraction bound values from *in vitro* binding assays. Error bars indicate errors given in Table 1. Data for 3064-B, 3064-BS, 3060-BS, 3060-B, and 3202-BS are from previously published data.[10] Open symbols indicate formulations for which there is pharmacokinetic data. (B) Spinal cord tissue exposure corrected score plotted against fraction bound values is shown. Error bars indicate the propagated error of the corrected score, which is the quotient of the remyelination score and AUC for spinal cord relative 3064-BS.

formulations were determined by incubating 230 nM aptamer in the presence of 0.2 μg/μL murine myelin suspension. Excess sheared salmon sperm DNA (20-fold by mass) was included as a competitor to suppress nonspecific binding. Final sample volume was 100 μL. Samples were incubated at 37°C for 90 min and then pelleted by centrifugation (microcentrifuge; 13,000 rpm; 1 min). The supernatant was collected and placed in a clean microfuge tube. The pellet was washed twice with PBS (with centrifugation) before being re-suspended in 100 μL PBS. The supernatant and wash samples were pooled. Pellet and non-pellet fractions were adjusted to an equal volume and placed in wells of a black 96-well microplate (Grenier Bio-One). The fluorescent aptamer signal was quantified using a plate reader (Analyst AD 96-384). Fraction bound values were calculated by determining the fraction of total fluorescent signal from the pellet sample. Control experiments showed that myelin did not quench oligonucleotide fluorescence. The effect size of myelin binding relative to 3064-B was calculated as follows: (mean of aptamer − mean of 3064-B)/(SD of 3064-B).

SUPPLEMENTAL INFORMATION

Supplemental Information includes three figures and can be found with this article online at https://doi.org/10.1016/j.omtm.2018.03.005.

AUTHOR CONTRIBUTIONS

Conceptualization, L.J.M., M.R., J.A.S., and A.E.W.; Methodology, L.J.M., M.R., J.A.S., R.M.H., and B.W.; Validation, R.M.H., J.A.S., and B.W.; Formal Analysis, R.M.H., J.P.P., and H.N.L.; Investigation, R.M.H. and H.N.L.; Resources, L.J.M. and M.R.; Writing – Original Draft, R.M.H. and H.N.L.; Writing – Review & Editing, R.M.H., L.J.M., and M.R.; Visualization, R.M.H. and J.P.P.; Supervision, L.J.M. and M.R.; Funding Acquisition, L.J.M., M.R., and A.E.W.

ACKNOWLEDGMENTS

This work was supported by generous funding from the Mayo Clinic and the Minnesota Partnership for Genomics and Biotechnology. We acknowledge technical support provided by Dr. Nicole Becker and Mabel Pierce for embedding all the spinal cord samples in plastics.

REFERENCES

1. Milo, R., and Miller, A. (2014). Revised diagnostic criteria of multiple sclerosis. Autoimmun. Rev. *13*, 518–524.
2. Lucchinetti, C., Brück, W., Parisi, J., Scheithauer, B., Rodriguez, M., and Lassmann, H. (2000). Heterogeneity of multiple sclerosis lesions: implications for the pathogenesis of demyelination. Ann. Neurol. *47*, 707–717.
3. Kantarci, O.H., Pirko, I., and Rodriguez, M. (2014). Novel immunomodulatory approaches for the management of multiple sclerosis. Clin. Pharmacol. Ther. *95*, 32–44.
4. Beer, S., Khan, F., and Kesselring, J. (2012). Rehabilitation interventions in multiple sclerosis: an overview. J. Neurol. *259*, 1994–2008.
5. De Stefano, N., Narayanan, S., Francis, G.S., Arnaoutelis, R., Tartaglia, M.C., Antel, J.P., Matthews, P.M., and Arnold, D.L. (2001). Evidence of axonal damage in the early stages of multiple sclerosis and its relevance to disability. Arch. Neurol. *58*, 65–70.
6. Murray, P.D., McGavern, D.B., Sathornsumetee, S., and Rodriguez, M. (2001). Spontaneous remyelination following extensive demyelination is associated with improved neurological function in a viral model of multiple sclerosis. Brain *124*, 1403–1416.
7. Douvaras, P., Wang, J., Zimmer, M., Hanchuk, S., O'Bara, M.A., Sadiq, S., Sim, F.J., Goldman, J., and Fossati, V. (2014). Efficient generation of myelinating oligodendrocytes from primary progressive multiple sclerosis patients by induced pluripotent stem cells. Stem Cell Reports *3*, 250–259.
8. Warrington, A.E., Bieber, A.J., Ciric, B., Pease, L.R., Van Keulen, V., and Rodriguez, M. (2007). A recombinant human IgM promotes myelin repair after a single, very low dose. J. Neurosci. Res. *85*, 967–976.
9. Smestad, J., and Maher, L.J., 3rd (2013). Ion-dependent conformational switching by a DNA aptamer that induces remyelination in a mouse model of multiple sclerosis. Nucleic Acids Res. *41*, 1329–1342.
10. Nastasijevic, B., Wright, B.R., Smestad, J., Warrington, A.E., Rodriguez, M., and Maher, L.J., 3rd (2012). Remyelination induced by a DNA aptamer in a mouse model of multiple sclerosis. PLoS ONE *7*, e39595.
11. Rodriguez, M., Oleszak, E., and Leibowitz, J. (1987). Theiler's murine encephalomyelitis: a model of demyelination and persistence of virus. Crit. Rev. Immunol. *7*, 325–365.
12. Zadeh, J.N., Wolfe, B.R., and Pierce, N.A. (2011). Nucleic acid sequence design via efficient ensemble defect optimization. J. Comput. Chem. *32*, 439–452.
13. Yin, P., Choi, H.M., Calvert, C.R., and Pierce, N.A. (2008). Programming biomolecular self-assembly pathways. Nature *451*, 318–322.
14. Elmén, J., Thonberg, H., Ljungberg, K., Frieden, M., Westergaard, M., Xu, Y., Wahren, B., Liang, Z., Ørum, H., Koch, T., and Wahlestedt, C. (2005). Locked nucleic acid (LNA) mediated improvements in siRNA stability and functionality. Nucleic Acids Res. *33*, 439–447.
15. Perschbacher, K., Smestad, J.A., Peters, J.P., Standiford, M.M., Denic, A., Wootla, B., Warrington, A.E., Rodriguez, M., and Maher, L.J., 3rd (2015). Quantitative PCR analysis of DNA aptamer pharmacokinetics in mice. Nucleic Acid Ther. *25*, 11–19.